

Instability and Momentum Bifurcation of a molecular BEC in a Shaken Lattice with Exotic Dispersion

Kaiyue Wang, Feng Xiong, Yun Long, Yun Ma, Colin V. Parker
School of Physics, Georgia Institute of Technology, Atlanta, Georgia 30332, USA
(Dated: April 18, 2023)

We place a molecular Bose-Einstein condensate in a 1D shaken lattice with a Floquet-engineered dispersion, and observe the dynamics in both position and momentum space. At the initial condition of zero momentum, our engineered dispersion is inverted, and therefore unstable. We observe that the condensate is destabilized by the lattice shaking as expected, but rather than decaying incoherently or producing jets, as in other unstable condensates, under our conditions the condensate bifurcates into two portions in momentum space, with each portion subsequently following semiclassical trajectories. We can model the evolution with a Gross-Pitaevskii equation, which suggests the origin of the bifurcation lies in the development of relatively long-wavelength density corrugation. We propose that this relatively clean bifurcation in momentum space has application for counter-diabatic preparation of exotic ground states in many-body quantum simulation schemes.

Degenerate quantum gases of ultracold atoms have emerged as powerful simulators of both equilibrium and non-equilibrium properties. One method of non-equilibrium simulation is to prepare Bose-Einstein condensates (BECs) with initial conditions far from the ground state and study the resulting dynamics. In some cases, the nominally unstable point can in fact be at least quasi-stable, such as the recently observed soliton in an inverted band[1] or many-body scar states [2] which lead to anomalously long lifetimes for spin helices[3]. In other cases, dramatic types of decay can be observed such as the so-called Bose-Nova [4] and Bose Fireworks [5]. Of course, conventional thermalization can also occur. Motivated by these exciting possibilities, we investigate the dynamics of strongly interacting 3D molecular BECs (mBECs) of ${}^6\text{Li}_2$ exposed to a shaken optical lattice along one dimension. The shaken lattice is a well-known technique capable of modifying the energy-momentum dispersion relation of the system's effective Hamiltonian [6, 7]. It has been used, for example, to study the formation of density waves[8] and spin dependent tunneling effects[9]. Most notably, a double-well feature can be generated, featuring an unstable point at the Brillouin zone center and two stable minima at tunable locations in the zone[10]. Distinct from previously observed dynamics in similar systems[1, 11], we observe that condensates initially at the unstable point break apart into two distinct portions (bifurcation), rather than decaying into multiple fragments or forming many local domains. This is surprising since in the Kibble-Zurek picture, rapid quenches form many domains with short correlation length, rather than a few large domains. Nevertheless, we can model the dynamics with a numerical Gross-Pitaevskii Equation (GPE), yielding results in qualitative agreement with observations. The stability of the mBEC in the process provides inspiration for designing protocols to load strongly-interacting BECs or degenerate Fermi gases into exotic band shapes generated by shaken lattices or other methods in a counter-diabatic

approach.

These dynamics represent a first step towards using shaken lattices with degenerate Fermi gases or molecular BECs, where exotic band shape such as the double-well may change or induce instability to the Fermi surface, and Cooper pairing outside the classical BCS description may occur. However, so far, little experimental work has been published with ultracold Fermi gases in exotic band shapes generated through shaken lattice, but similar effects have been achieved with spin-orbit coupling (SOC) or Zeeman-field-induced spin imbalance [12]. Proposals have been made for generating complex Fermi surfaces [13] or realizing Fulde-Ferrell-Larkin-Ovchinnikov (FFLO) phases, which are challenging to observe [14–16], but predicted to be more stable in the shaken lattice [17, 18]. Even outside of Fermi gases the shaken lattice technique reveals interesting behavior in “dispersion engineering” [19], allowing dispersion minima with tunable separation [11, 20, 21], and balance [10, 22]. The ground states of Bose-Einstein condensates (BEC) at the bottom of either dispersion minimum makes an analogy to spin one-half systems and their occupation can be read out through time-of-flight (TOF) imaging and domain reconstruction [10]. The adiabatic or nearly adiabatic evolution of the system during a change in ground state dispersion has offered insight into features of general phase transitions such as scaling laws near critical points [11], domains and domain wall dynamics [10, 22], and artificial gauge fields [20]. Alternatively, an inverted band can be achieved with strong off-resonance shaking enabling studies of discontinuous phase transitions [23].

Our experiment uses an ultracold molecular BEC (mBEC) of ${}^6\text{Li}_2$ and an 1D optical lattice (OL) created by a retro-reflected beam of wavelength $\lambda_L = 1064\text{ nm}$, (lattice constant $a_L = 532\text{ nm}$). We name the lattice direction the z axis. The lattice's returning beam is diffracted by a pair of acousto-optic modulators (AOM) in a double-pass configuration. One of the AOM input signals is modulated by an IQ modulator, where we

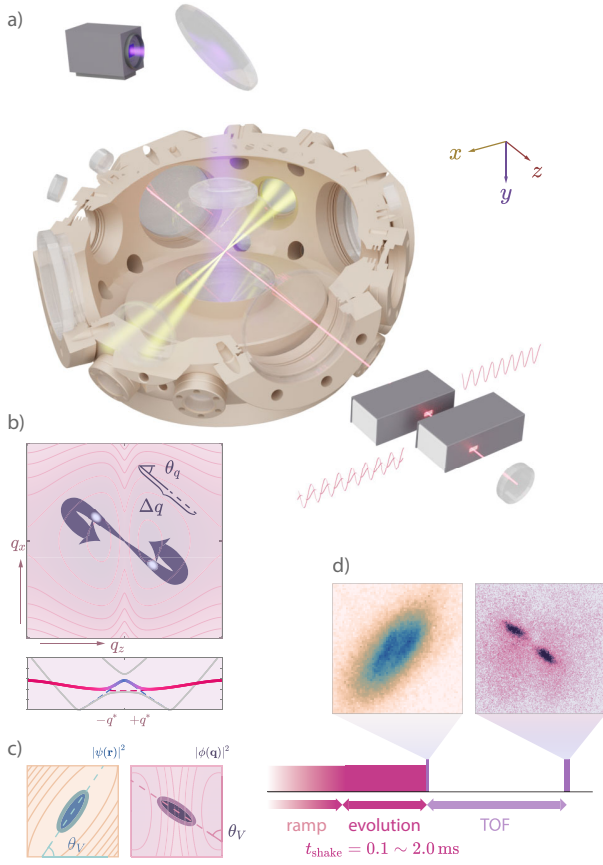


FIG. 1. **a** An illustration of the experimental setup. The ${}^6\text{Li}_2$ mBEC is loaded into the lattice (red) and a crossed pair of dipole traps (yellow), the imaging (violet) direction y is perpendicular to the plane of dipole traps and lattice. The lattice beam passes twice through each of the two AOMs, one of which has the input signal modulated to create a shaken lattice. **b** Effective dispersion in the $x-z$ plane. The arrows indicate a typical symmetric trajectory of the center-of-mass of each cluster of molecules. The clusters' locations can be characterized by the distance parameter Δq and angle θ_q . The line cut below shows the dispersion of quasienergy along the z axis. The colored solid curve has the double-well feature, and is a hybrid of the ground band (red) and 2nd band (blue) from the non-shaken dispersion (dashed). **c** Illustration of the initial profile in position and momentum space, with the contour lines depicting the potential and the dispersion close to the zone center. **d** Typical observations from the experiment: an in-situ image taken at the end of the shaking period, and a time-of-flight (TOF) image, reflecting the momentum space distribution.

mix in the shaking signal. We characterize the shaking by the quadrature component's oscillation angular frequency ω and its maximum amplitude relative to the static in-phase component ξ_{\max} . This description is only approximate, however, due to the double-passing of the AOM (see supplemental material). The system can be

described by a time-dependent Hamiltonian density

$$\mathcal{H} = \bar{\psi} \left[-\frac{\hbar^2 \nabla^2}{2m} - \mu \right] \psi + [V_L(t) + V_{\text{trap}}] \bar{\psi} \psi + \frac{g}{2} (\bar{\psi} \psi)^2, \quad (1)$$

where m is the mass of ${}^6\text{Li}_2$ molecules, ψ is the bosonic annihilation operator, μ the chemical potential, and g the interaction strength. The lattice potential contains

$$V_L(t) = V_L \left[\cos(2q_L z) + \xi_{\max} \cos\left(2q_L z + \frac{\pi}{2}\right) \cos(\omega t) \right] \quad (2)$$

V_{trap} represents the trapping potential, $V_L = 2.8E_R$, where $E_R = \frac{\hbar^2}{2m\lambda_L^2}$ is the recoil energy for ${}^6\text{Li}_2$ molecules, \hbar being the Planck constant and $q_L = \frac{2\pi}{\lambda_L}$ is the lattice light wavevector. The shaking of the lattice allows the first two lattice bands to couple, yielding an effective dispersion relation $D_{V_L, \omega, \xi_{\max}}(\mathbf{q})$, which can be calculated numerically from the shaking parameters [10]. The dispersion relation used for the majority of this work is shown in Fig. 1.

The details of our apparatus and the Fermi degenerate evaporation process have been described previously [24, 25]. We start by preparing a degenerate ${}^6\text{Li}_2$ molecular BEC of approximately 12000 molecules from a mixture of the ground the the first excited hyperfine states, through evaporative cooling in a crossed pair of dipole beams of wavelength 1070 nm, with the molecules bound by the Feshbach resonance. The mBEC is then adiabatically loaded into the optical lattice. The harmonic potential formed by both dipole traps and the lattice has trapping frequencies (210,500,810) Hz. Fig. 1 shows the experimental setup. The lattice shaking is ramped on over 1.2 ms (see supplemental material). To prepare most of the BEC in the ground band, the shaking frequency ramps from 80 kHz to the target value $\omega = 2\pi \times f$, with f between 45 kHz and 72 kHz, approximately matching the band gap between the lowest two Bloch bands at the zone center. At this point the condensate fraction is reduced to about 27%. The lattice shaking is maintained for a period of time t_{shake} , before the molecules are released from all traps and lattices. Our absorption imaging system records the optical density integrated along the y axis, which is perpendicular to the z axis and parallel to gravity.

When held in the lattice without shaking, the mBEC remains stable for more than 10 ms, its spatial profile $|\psi(\mathbf{r})|^2$ fitting the contour of the overall potential, which is of an elongated oval shape, with the long axis at an angle with the lattice beams by $\theta_V = 53^\circ$ (see Fig. 1c). If the shaking is turned on, the zone center becomes a saddle point, and the momentum space wavefunction $\phi(\mathbf{q})$ lies across both sides of the saddle. Under these conditions, instability develops due to the inverted dispersion, and with increasing time under modified dispersion relation, the condensate divides into two clusters in momentum space, each half having momentum in opposite

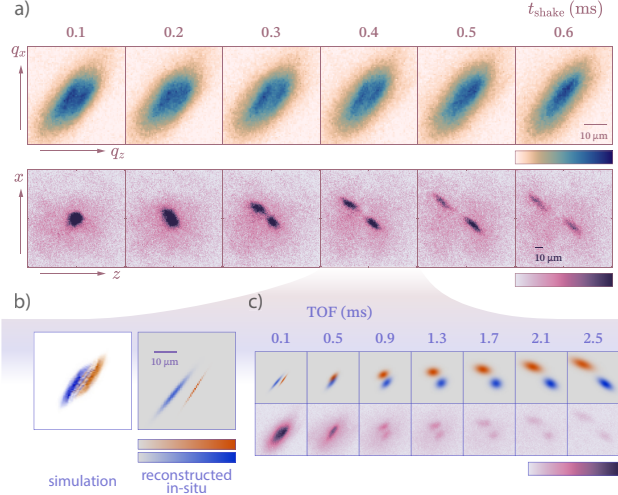


FIG. 2. **a** In-situ (top) and time-of-flight (bottom) images following shaking times t_{shake} from 0.1 ms to 0.6 ms. Data taken with $\xi_{\text{max}} = 0.5$, $f = 63$ kHz, lattice depth $V_L = 2.8E_R$. The image is cropped by the size of the first Brillouin zone. **b** colored simulation (left) and fitted in-situ data (right) showing the component with $+z$ momentum in red and that with $-z$ momentum in blue. For the simulation this is calculated by projecting the GP wavefunction onto $+z$ or $-z$ momentum states. For the in-situ data it is based on extrapolating backwards from the TOF progression in panel (c). **c** Expansion of the mBEC for varying TOF with $t_{\text{shake}} = 0.4$ ms. The upper row of panels shows a fit of two Gaussian distributions (resp. red and blue) to the data in the lower row of panels. All scale bars are $10 \mu\text{m}$.

directions along an axis approximately 45° from the lattice direction, close to the direction of strongest lattice confinement in the $x - z$ plane (see Fig. 2a). In real space, the condensate forms a low-density trench in the middle of the sample that can be resolved in in-situ images, see Fig. 2b. Observing over a variable time of flight (Fig. 2f), we see that the $-z$ side of the condensate moves back across the center and emerges traveling in the $+z$ direction, consistent with the inverted dispersion relation. That is, during the inverted dynamics prior to the time of flight, a portion of the condensate has acquired positive z momentum and become displaced in the $-z$ direction, while during the time of flight period it travels in the usual $+z$ direction. This can be confirmed by extrapolating the two clusters to their original positions (see supplemental material). The motion following lattice shaking is not entirely due to direct effects of the lattice, as the x direction has the unmodified dispersion, yet this half of the condensate also acquires momentum in the $-x$ direction. The other half of the condensate experiences the same effect with opposite signs. Our interaction strength can be characterized by an initial peak density of $6.9 \times 10^{12} \text{ cm}^{-3}$, and a molecule-molecule scattering length $a_{\text{MM}} = 0.6a = 491a_0$, where $a = 819a_0$ is the two-body scattering length at 650 G, a_0 is the Bohr

radius. The interaction strength may be one reason why our observed dynamics are different from experiments with weaker interactions as in [1]. It should also be noted that our static lattice depth is lower than in other experiments with near-resonant shaking[10, 11].

The two clusters move continuously in momentum space. We characterize the trajectory of the two clusters by their separation Δq and their relative angle to the z axis θ_q (See Fig. 1b). Subsequent evolution shows that the two clusters will overshoot beyond $\pm q^*$, where the dispersion slope is no longer inverted along z . In real space the two clusters also collide, corresponding to the vanishing of the trench in the in-situ profiles after 0.5 ms. At this point, a density wave could be forming at a wavevector corresponding to the separation Δq , whose wavelength $\sim 1.2 \mu\text{m}$ would be beyond our resolution limit of $2 \mu\text{m}$. After collision, we see loss of BEC density from heating and an imbalance of the clusters' molecule number. Although only a fraction of the wavefunction remains condensed, we can still distinguish the two clusters up to 2.0 ms of evolution, when the clusters appear to end up around the potential minima $\pm q^*$.

We performed numeric simulation using a model with an effective dispersion $\hat{D}_{V_L, \omega, \xi_{\text{max}}}(\mathbf{q})$ (see Fig. 3). The evolution of the BEC wavefunction $\psi(\mathbf{r})$ can be described by the non-linear Gross-Pitaevskii equation derived from (1):

$$i\hbar \frac{\partial \psi}{\partial t} = \left\{ -\frac{\hbar^2 \nabla^2}{2m} + V_{\text{trap}}(\mathbf{r}) + g|\psi^2| + V_L \left[\cos(2q_L z) + \xi(t) \cos\left(2q_L z + \frac{\pi}{2}\right) \right] \right\} \psi, \quad (3)$$

where $\xi(t) = \xi_{\text{max}} \cos(\omega t)$. The Hamiltonian is periodic in time with period $T = \frac{2\pi}{\omega}$. Floquet theory tells us that the solution to equation (3) will be in the form $|\psi(t)\rangle = \sum_n a_n |u_n(t)\rangle e^{-i\epsilon_n t/\hbar}$, where $|u_n(t)\rangle$ are the fast-changing Floquet modes. Each mode is t -dependent and periodic in T . The method separates the evolution into a fast-repeating micro-motion $|u_n(t)\rangle$ and the slow-evolving dynamic ϵ_n . The latter of these is where our interest mainly lies, which is described by the effective Hamiltonian (4).

$$\hat{H}_{\tau_0, \text{Floq}} = \frac{i\hbar}{T} \log \hat{U}(\tau_0, \tau_0 + T) \quad (4)$$

$$\approx \frac{i\hbar}{T} \log \prod_{\tau_0}^{\tau_0+T} \exp \left\{ -\frac{i}{\hbar} \left[\hat{K} + \hat{V}_0 + \hat{V}_{\frac{\pi}{2}} \xi(t) \right] dt \right\} + \hat{V}_{\text{trap}} + g|\psi^2| \quad (5)$$

$$\approx \hat{D}_{V_L, \omega, \xi_{\text{max}}} + \hat{V}_{\text{trap}} + g|\psi^2| \quad (6)$$

We perform a Trotter expansion, and take advantage of the fact that the fast changing term in \hat{H} , which is the shaken lattice term, will couple mostly with the kinetic term. In (6), \hat{K} is the kinetic energy operator, \hat{V}_0 and $\hat{V}_{\frac{\pi}{2}}$ are lattice operators for lattices with the

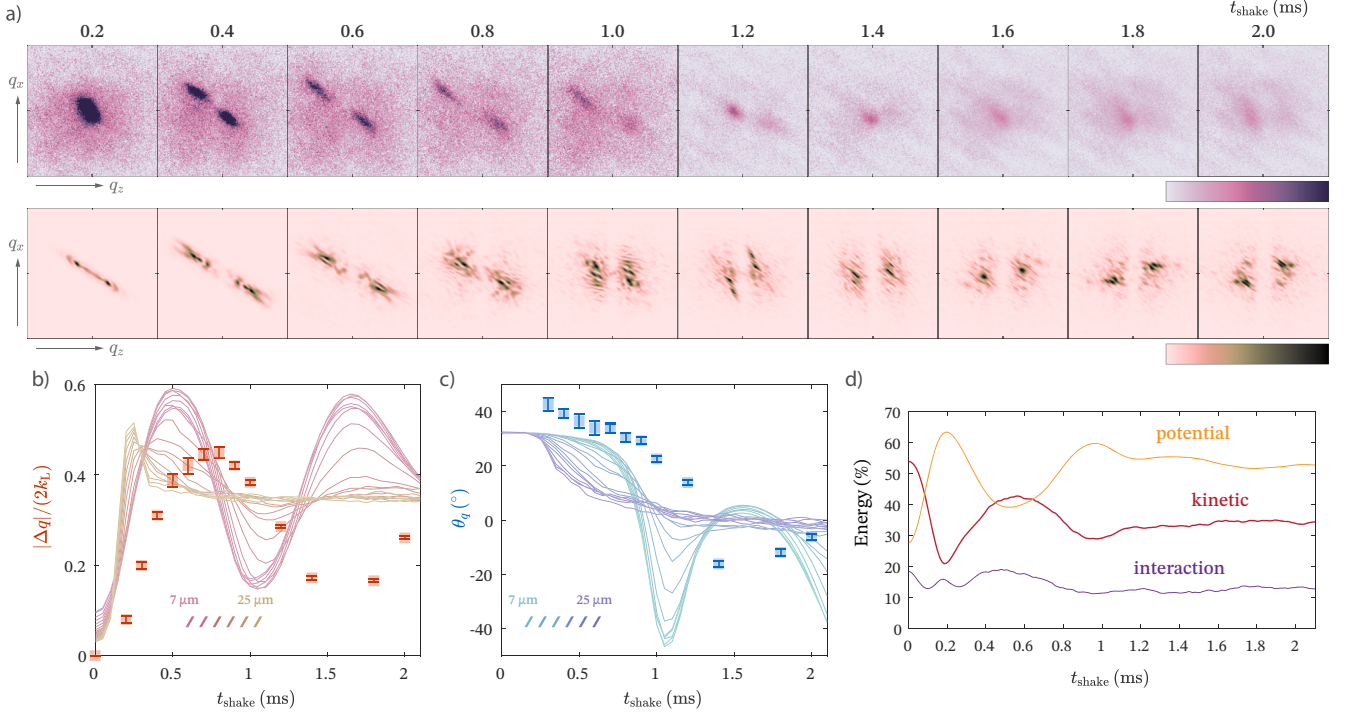


FIG. 3. **a** Evolution of the momentum distribution, the top row is obtained by TOF imaging, for shaking times $t_{\text{shake}} = 0.2 \text{ ms} \sim 2.0 \text{ ms}$, the bottom row is from simulation under similar conditions. **b** Measurement of the peak separation Δq between the two clusters (points with error bars), together with the corresponding value from GP simulations (solid lines). The lines correspond to results of the simulation with a range of initial sizes. **c** Measurement and GP simulation results for the angle of separation, θ_q . **d** Evolution of the kinetic energy (red), trap potential energy (yellow), and interaction energy (violet) from one of the simulations. The simulation data in (a) and (c) use initial cloud size $16 \mu\text{m}$.

same depth V_L at phase 0 and $\frac{\pi}{2}$, representing the static lattice and shaken lattice respectively. $\hat{D}_{V_L, \omega, \xi_{\text{max}}}$ is the effective dispersion operator resulting from the kinetic energy, lattice, and lattice shaking, calculated numerically through the Trotter expansion in (5). At moderate shaking amplitude and when the shaking frequency matches the band gap, the lowest three bands from the static lattice hybridize around the zone center, maintaining the feature of the peak from the second band, with a local minimum on each side.

Our simulation starts at the approximate ground state with $V_L = 0$, where the initial wavefunction is generated by $\psi(t=0) = \sqrt{-V_{\text{trap}}/g}$. We then take a Trotter product of $\exp\{-i\hat{D}\Delta t/\hbar\}$ and $\exp\{-i(\hat{V}_{\text{trap}} + g|\psi|^2)\Delta t/\hbar\}$ by calculating their matrix representations in momentum space and position space respectively (see supplemental material). Unfortunately, the single-band GP method fails to capture the interaction that exists between higher band states and the ground band, that is it assumes the ground-to-first excited transition frequency is not affected by interactions. In reality this frequency, or equivalently the phase velocity of acoustic waves with the period of the lattice spacing, is shifted for strongly

interacting systems. To correct for this, we introduce a modified recoil energy E'_R acquired from the measured phase velocity in a Kapitza-Dirac experiment, which is about 10 % larger than the E_R calculated from the molecular mass. This is consistent with the observation that the shaking frequency threshold for creating a momentum bifurcation is generally larger than the free particle band gap would allow (See Fig. 4).

Comparing $\phi(\mathbf{q})$ in experiment and simulation under the same nominal conditions (Fig. 3), both show the same trend of bifurcation and a similar subsequent trajectory. However, the simulation predicts a slightly more rapid initial splitting, and for $t_{\text{shake}} \geq 1.0 \text{ ms}$, after fractions collide in real space, the simulation shows a weaker damping effect, with Δq and θ_q oscillating multiple times. Although experimentally the size along the z axis is $23 \mu\text{m}$, simulations with smaller initial condensate sizes come closer to matching the experimental timescale, which may be explained by the low condensate fraction if the condensate is assumed to occupy a smaller central region of the observed in-situ density profile. Similarly, the higher damping in the experiment versus the simulation may arise from collisions with the thermal background.

By tuning the shaking frequency ω we effectively change how much the second band protrudes into the

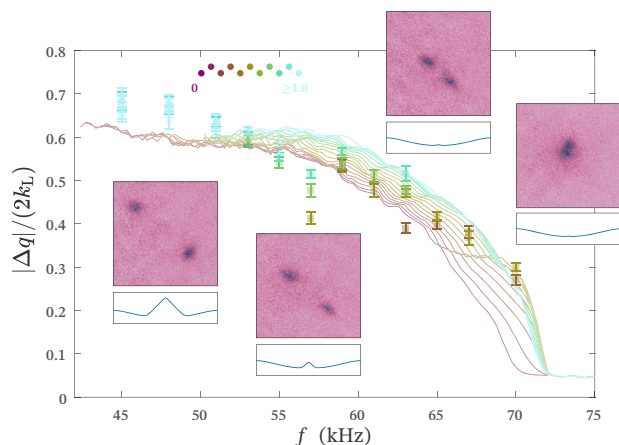


FIG. 4. Variation of the peak separation Δq at $t_{\text{shake}} = 0.4$ ms for a range of shaking frequencies from $f = 45 \sim 72$ kHz (data points with error bars) together with results from the GP simulation (solid lines). The inset images are TOF momentum distributions from which Δq is determined, together with the calculated dispersion appropriate to that frequency (from left to right: 48, 63, 70, 72 kHz). The color of the lines and data points indicate different shaken amplitudes ξ_{max} .

ground band in the Floquet picture, and the separation between the quasienergy minima $2|q^*|$. At lower frequencies, the momentum space clusters glide along a longer slope and exhibits larger separation Δq at the same t_{shake} . At higher frequencies, the target band is not hybridized and $q^* = 0$, the bifurcation will thus not happen. Figure 4 displays the evolution at a range of f , which matches our simulation results. Increasing the amplitude of the shaking does not change the band shape significantly for the conditions of our experiment, and therefore does not effect the simulation results. However, experiments with stronger shaking can exhibit heating and are more difficult to interpret.

In conclusion, we have successfully loaded a strongly interacting $^6\text{Li}_2$ molecular BEC into a shaken lattice, with a Floquet engineered double-well dispersion. The resulting dynamics differs significantly from previous observations, featuring a bifurcation into two clusters in momentum space and a trench in the position space density. We can describe the dynamics semi-classically and model it qualitatively with a Gross-Pitaevskii simulation. We show that this phenomenon occurs over a substantial range of dispersion relations tuned via the lattice shaking frequency. The rapid splitting into two clusters suggests a novel method for preparing molecular-Bose or Fermi systems in non-equilibrium states with exotic engineered dispersions. For example, if after the initial splitting, conditions could be altered by the appropriate counter-diabatic protocol, one might produce a “soft-landing” for the two clusters leaving them as quasi-stable domains. In such a way even strongly interacting systems, such as

unitary Fermi gases, might be prepared in domain configurations that couldn’t be achieved adiabatically due to unwanted collisional heating [26–28].

We acknowledge funding from NSF CAREER award No. 1941985. We also thank Carlos Sa de Melo for comments on the manuscript.

-
- [1] M. Mitchell, A. Di Carli, G. Sinuco-León, A. La Rooij, S. Kuhr, and E. Haller, Floquet solitons and dynamics of periodically driven matter waves with negative effective mass, *Physical Review Letters* **127**, 243603 (2021).
 - [2] M. Serbyn, D. A. Abanin, and Z. Papić, Quantum many-body scars and weak breaking of ergodicity, *Nature Physics* **17**, 675 (2021).
 - [3] P. N. Jepsen, Y. K. E. Lee, H. Lin, I. Dimitrova, Y. Margalit, W. W. Ho, and W. Ketterle, Long-lived phantom helix states in heisenberg quantum magnets, *Nature Physics* **18**, 899 (2022).
 - [4] T. Lahaye, J. Metz, B. Froehlich, T. Koch, M. Meister, A. Griesmaier, T. Pfau, H. Saito, Y. Kawaguchi, and M. Ueda, d-wave collapse and explosion of a dipolar bose-einstein condensate, *Physical review letters* **101**, 080401 (2008).
 - [5] L. W. Clark, A. Gaj, L. Feng, and C. Chin, Collective emission of matter-wave jets from driven bose-einstein condensates, *Nature* **551**, 356 (2017).
 - [6] A. Eckardt, Colloquium: Atomic quantum gases in periodically driven optical lattices, *Reviews of Modern Physics* **89**, 011004 (2017).
 - [7] C. Weitenberg and J. Simonet, Tailoring quantum gases by floquet engineering, *Nature Physics* **17**, 1342 (2021).
 - [8] H. P. Zahn, V. P. Singh, M. N. Kosch, L. Asteria, L. Freystatzky, K. Sengstock, L. Mathey, and C. Weitenberg, Formation of spontaneous density-wave patterns in dc driven lattices, *Phys. Rev. X* **12**, 021014 (2022).
 - [9] J. Struck, J. Simonet, and K. Sengstock, Spin-orbit coupling in periodically driven optical lattices, *Phys. Rev. A* **90**, 031601 (2014).
 - [10] C. V. Parker, L.-C. Ha, and C. Chin, Direct observation of effective ferromagnetic domains of cold atoms in a shaken optical lattice, *Nature Physics* **9**, 769 (2013).
 - [11] L. W. Clark, L. Feng, and C. Chin, Universal space-time scaling symmetry in the dynamics of bosons across a quantum phase transition, *Science* **354**, 606 (2016).
 - [12] J. J. Kinnunen, J. E. Baarsma, J.-P. Martikainen, and P. Törmä, The fulde-ferrell-larkin-ovchinnikov state for ultracold fermions in lattice and harmonic potentials: a review, *Reports on Progress in Physics* **81**, 046401 (2018).
 - [13] A. Keleş, E. Zhao, and W. V. Liu, Effective theory of interacting fermions in shaken square optical lattices, *Physical Review A* **95**, 063619 (2017).
 - [14] Y.-a. Liao, A. S. C. Rittner, T. Paprotta, W. Li, G. B. Partridge, R. G. Hulet, S. K. Baur, and E. J. Mueller, Spin-imbalance in a one-dimensional fermi gas, *Nature* **467**, 567 (2010).
 - [15] G. B. Partridge, W. Li, R. I. Kamar, Y. an Liao, and R. G. Hulet, Pairing and phase separation in a polarized fermi gas, *Science* **311**, 503 (2006), <https://www.science.org/doi/pdf/10.1126/science.1122876>.

- [16] B. A. Olsen, M. C. Revelle, J. A. Fry, D. E. Sheehy, and R. G. Hulet, Phase diagram of a strongly interacting spin-imbalanced fermi gas, *Phys. Rev. A* **92**, 063616 (2015).
- [17] Z. Zheng, C. Qu, X. Zou, and C. Zhang, Floquet fulde-ferrell-larkin-ovchinnikov superfluids and majorana fermions in a shaken fermionic optical lattice, *Physical Review A* **91**, 063626 (2015).
- [18] Z. Zheng, C. Qu, X. Zou, and C. Zhang, Fulde-ferrell superfluids without spin imbalance in driven optical lattices, *Physical review letters* **116**, 120403 (2016).
- [19] K. Sandholzer, A.-S. Walter, J. Minguzzi, Z. Zhu, K. Viebahn, and T. Esslinger, Floquet engineering of individual band gaps in an optical lattice using a two-tone drive, *Phys. Rev. Res.* **4**, 013056 (2022).
- [20] S. Erne, R. Bückler, T. Gasenzer, J. Berges, and J. Schmiedmayer, Universal dynamics in an isolated one-dimensional bose gas far from equilibrium, *Nature* **563**, 225 (2018).
- [21] B. M. Anderson, L. W. Clark, J. Crawford, A. Glatz, I. S. Aranson, P. Scherpelz, L. Feng, C. Chin, and K. Levin, Direct lattice shaking of bose condensates: Finite momentum superfluids, *Physical review letters* **118**, 220401 (2017).
- [22] K.-X. Yao, Z. Zhang, and C. Chin, Domain-wall dynamics in bose-einstein condensates with synthetic gauge fields, *Nature* **602**, 68 (2022).
- [23] B. Song, S. Dutta, S. Bhave, J.-C. Yu, E. Carter, N. Cooper, and U. Schneider, Realizing discontinuous quantum phase transitions in a strongly correlated driven optical lattice, *Nature Physics* **18**, 259 (2022).
- [24] Y. Long, F. Xiong, V. Gaire, C. Caligan, and C. V. Parker, All-optical production of Li 6 molecular Bose-Einstein condensates in excited hyperfine levels, *Physical Review A* **98**, 043626 (2018).
- [25] Y. Long, F. Xiong, and C. V. Parker, Spin susceptibility above the superfluid onset in ultracold fermi gases, *Physical Review Letters* **126**, 153402 (2021).
- [26] S. Choudhury and E. J. Mueller, Stability of a floquet bose-einstein condensate in a one-dimensional optical lattice, *Physical Review A* **90**, 013621 (2014).
- [27] S. Choudhury and E. J. Mueller, Stability of a bose-einstein condensate in a driven optical lattice: Crossover between weak and tight transverse confinement, *Physical Review A* **92**, 063639 (2015).
- [28] S. Choudhury and E. J. Mueller, Transverse collisional instabilities of a bose-einstein condensate in a driven one-dimensional lattice, *Physical Review A* **91**, 023624 (2015).

Instability and Momentum Bifurcation of a molecular BEC in a Shaken Lattice with Exotic Dispersion

Kaiyue Wang, Feng Xiong, Yun Long, Yun Ma, Colin V. Parker

School of Physics, Georgia Institute of Technology, Atlanta, Georgia 30332, USA

(Dated: April 18, 2023)

arXiv:2304.07423v1 [cond-mat.quant-gas] 14 Apr 2023

SHAKING SCHEME

One of the double-passed AOMs for the retro-reflected lattice beam has a modulated signal to create the shaking. The unmodified signal $s = s_{\max} \cos(2\pi\nu t)$ goes through an IQ modulator as shown in the diagram on the left of Fig. S1. The IQ modulator takes the signal and divides it into two components: an in-phase lattice component (created by a DC voltage on the “Q” channel of the IQ modulator), and an oscillating quadrature component that has the phase retarded by $\pi/2$ (created by an AC voltage on the “I” channel). Note that the usage of I and Q is reversed from typical configuration, although they are equivalent for our purposes. The input signal to the AOM, s' , is the mixing of the two components with tunable amplitudes. We set the relative amplitude of Q to be 1, and I to be $\zeta(t) = -\zeta_{\max} \cos(\omega t)$. Therefore,

$$s' = s_{\max} \left[1 \times \cos(2\pi\nu t) - \zeta(t) \times \cos\left(2\pi\nu t - \frac{\pi}{2}\right) \right], \quad (1)$$

or in terms of complex amplitudes,

$$\tilde{s}' = (1 - i\zeta(t))\tilde{s}. \quad (2)$$

In the right figure, the bottom diagram shows an exaggerated version of the two components (“I” in red, “Q” in blue). The upper diagram shows the mixed signal s' in violet, and the unmodified s (blue) as a reference. As can be seen the modulation is in both phase and amplitude.

Consider the change of complex amplitude for the lattice light, which passes through the modulated AOM twice in the same order, and the unmodulated AOM (also with input frequency ν , in our case $\nu = 80$ MHz) twice in the opposite order. For every pass

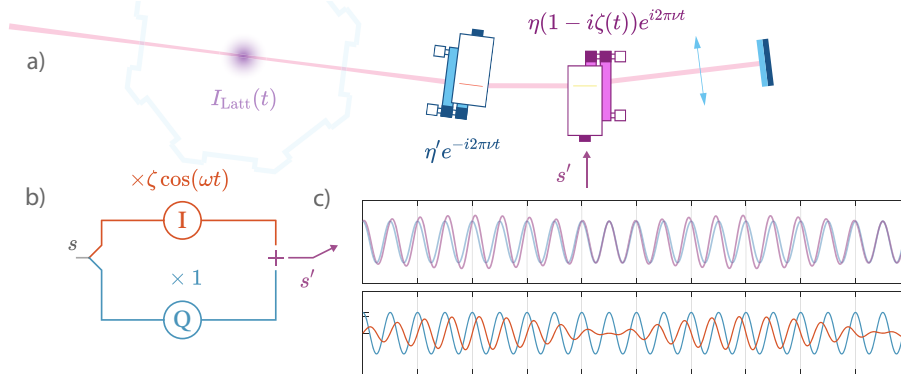


FIG. S1. Experimental configuration for lattice shaking with a doubled-passed AOM.

of the modulated AOM, it gains a complex factor of $\tilde{\eta}_+ = \eta(1 - i\zeta(t))e^{-i2\pi\nu t}$, and for the unmodulated AOM a factor of $\tilde{\eta}_- = \eta'e^{i2\pi\nu t}$. Here, η and η' are the real efficiencies for amplitudes. The retro-reflected beam in the chamber thus carries a factor of $\tilde{\eta} = \tilde{\eta}_+^2 \tilde{\eta}_-^2 = \eta^2 \eta'^2 (1 - 2i\zeta(t) - \zeta(t)^2)$.

We now calculate the light intensity at the center of the chamber. Assuming the incoming light has a complex amplitude of $\tilde{A}_{\text{inc}}(t) = Ae^{ikz}e^{-ikt}$, the retro-reflected light has complex amplitude of $\tilde{A}_{\text{retro}}(t) = Ae^{-ikz}e^{-ikt}\tilde{\eta}$. The intensity is,

$$\begin{aligned} I(t) &= \left| \tilde{A}_{\text{inc}} + \tilde{A}_{\text{retro}} \right|^2 = \left(\tilde{A}_{\text{inc}}^* + \tilde{A}_{\text{retro}}^* \right) \left(\tilde{A}_{\text{inc}} + \tilde{A}_{\text{retro}} \right) \\ &= \left| \tilde{A}_{\text{inc}} \right|^2 + \left| \tilde{A}_{\text{retro}} \right|^2 + 2 \text{Re} \tilde{A}_{\text{inc}} \tilde{A}_{\text{retro}}^* \end{aligned} \quad (3)$$

Only the third term contains spatial modulations and serves as an optical lattice. The intensity is

$$\begin{aligned} I_{\text{Latt}}(t) &= 2 \text{Re} \tilde{A}_{\text{inc}} \tilde{A}_{\text{retro}}^* = 2A^2\eta^2\eta'^2 \text{Re} \left[e^{2ikz} (1 - \zeta(t)^2 + i2\zeta(t)) \right] \\ &= 2I_{\text{max}} \left[(1 - \zeta(t)^2) \cos(2kz) + 2\zeta(t) \cos\left(2kz + \frac{\pi}{2}\right) \right] \\ &\approx 2I_{\text{max}} \left[\cos(2kz) + \xi_{\text{max}}(t) \cos\left(2kz + \frac{\pi}{2}\right) \cos(\omega t) \right], \end{aligned} \quad (4)$$

corresponding to an in-phase lattice component with amplitude $1 - \zeta(t)^2$ close to the unmodulated static lattice and a $\pi/2$ shifted lattice component with amplitude $2\zeta(t)$. At lower maximum signal amplitudes ζ_{max} , the shifted lattice oscillates at double the lattice amplitude: $\xi_{\text{max}} = 2\zeta_{\text{max}}$. The small modulation of lattice intensity at twice the shaking frequency can be neglected to a good approximation. For example, if $\xi_{\text{max}} = 1/2$, then $\zeta_{\text{max}} = 1/4$, and $\zeta^2(t) = [1 + \cos(2\omega t)]/32$.

SEQUENCE DETAILS

Figure S2 below shows the sequence of each experimental run. First, the incoming lattice beam is turned on adiabatically in 99 ms. The mBEC's OD profile is shown on the top left of the diagram, and serves as the initial condition of the evolution, yielding the initial size parameters and θ_V . Second, the retro-reflected beam is turned on over 1 ms by ramping up the signal to the pair of AOMs, and the incoming lattice beam is weakened to maintain the overall average intensity. Then, the IQ modulation that produces the shaking is ramped up over 0.1 ms, and the frequency of the IQ modulation is ramped down from 80 kHz to

the target f over another 0.1 ms (reflected as the tone change in the shading in the figure). This enables the mBEC to be loaded onto the desired hybridized band. Next, with constant shaking frequency and amplitude ω and ξ_{\max} , the mBEC evolves for a controlled period of time t_{shake} . Starting from the final 5 ms of the lattice beam turn-on, the magnetic field is kept at 650 G, far on the BEC-side of resonance, where Feshbach molecules are bound. Finally, the destructive imaging pulse can be taken at multiple possible times. In-situ images are taken directly at the end of the shaking time. In order to minimize the motion of atoms during the pulse this requires the shortest possible pulse, which for our experiment is 1 μs , and to reduce shot noise the image is averaged over 100 shots. The imaging frequency is chosen by optimizing the optical density of the weakly-bound molecules, which may break apart during the pulse. For short TOF images, within 0.1 ms to 1 ms after release of the trap, a longer 100 μs imaging pulse can be used. For longer TOF images, we can afford to ramp the magnetic field closer to the resonance, where the Feshbach pairs are less tightly bound and easier to image. A long TOF image that resolves the momentum distribution is typically taken at 3 ms.

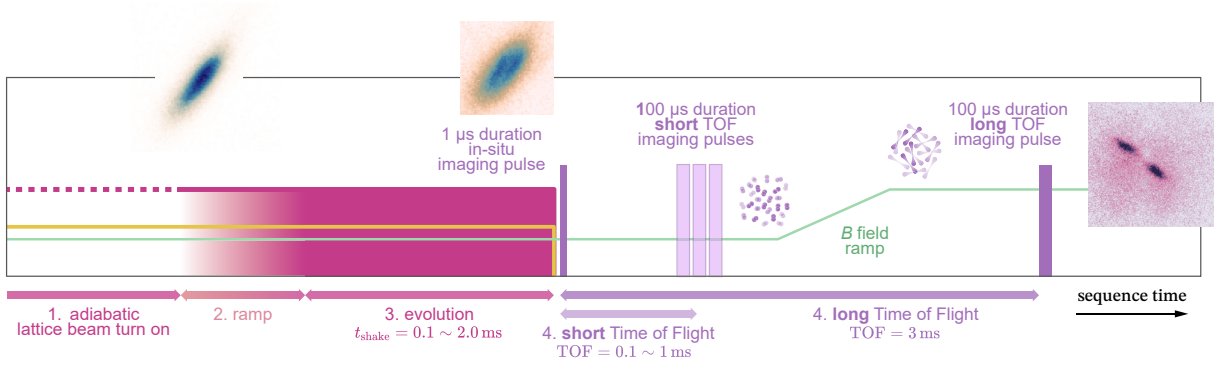


FIG. S2. Experimental sequence (see description in the supplemental text).

EXTRAPOLATION

To reconstruct the in-situ distribution from short TOF images, we fit each TOF image with the sum of two 2D-Gaussian peaks, each of which is allowed to have an arbitrary

rotation angle and asymmetric long/short radius:

$$f(R) = f_+(R) + f_-(R)$$

$$f_{\pm}(R) = A_{\pm} \exp \left\{ -\frac{1}{2} (R - \mu_{\pm})^T \Sigma_{\pm}^{-1} (R - \mu_{\pm}) \right\} \quad (5)$$

For conciseness we shall not label \pm when introducing the following symbols and focus on only one of the peaks. Here, $R = \begin{pmatrix} x \\ z \end{pmatrix}$ is the 2D positional vector, $\mu = \begin{pmatrix} \mu_x \\ \mu_z \end{pmatrix}$ is the center of the corresponding Gaussian peak, $\Sigma^{-1} = U^T \begin{pmatrix} \frac{1}{\sigma_1^2} & \\ & \frac{1}{\sigma_2^2} \end{pmatrix} U$ is the scaling matrix, where $U = \begin{pmatrix} \cos \theta & -\sin \theta \\ \sin \theta & \cos \theta \end{pmatrix}$ is the rotation matrix, and $\sigma_{1,2}$ are the two size parameters in length units, representing the Gaussian radius along the long and short axis. Of course, we need to make sure that the two peaks in each image are selected consistently.

To extrapolate to the *in-situ* time t_0 from other two known time points t_{α} and t_{β} , we assume the peaks' distribution follows an optimal transportation [1]:

$$\Sigma(\tau) = [(1 - \tau)\mathbb{1} + \tau A_{\alpha;\beta}] \Sigma_{\alpha} [(1 - \tau)\mathbb{1} + \tau A_{\alpha;\beta}] \quad (6)$$

Here, $\tau = \frac{t - t_{\alpha}}{t_{\beta} - t_{\alpha}}$ is the normalized time, so that $\Sigma(0) = \Sigma_{\alpha}$, $\Sigma(1) = \Sigma_{\beta}$. and $A_{\alpha;\beta}$ is the transportation matrix given by

$$A_{\alpha;\beta} = \Sigma_{\alpha}^{-\frac{1}{2}} \left(\Sigma_{\alpha}^{\frac{1}{2}} \Sigma_{\beta} \Sigma_{\alpha}^{\frac{1}{2}} \right)^{\frac{1}{2}} \Sigma_{\alpha}^{-\frac{1}{2}} \quad (7)$$

The inverse and square root of the Σ matrices are well-defined since they can be diagonalized through 2D-rotations. The peaks in the constructed in-situ image is acquired by choosing $t_{\alpha} = 0.8 \text{ ms}$ and $t_{\beta} = 2.5 \text{ ms}$, then taking in $\tau = \frac{t_0 - t_{\alpha}}{t_{\beta} - t_{\alpha}}$.

SIMULATION SCHEME

The simulation is run through a MATLAB application. The wavefunction is represented by a complex 3D-array $\psi(x, y, z)$, typically of size $100 \times 10 \times 100$. We choose the resolution in the lattice direction z to be exactly $\lambda_L/2$, so that the discrete Fourier transform of the wavefunction fills one Brillouin zone along z . At each step of evolution, we calculate the phase accumulation at each site by multiplying $i(V_{\text{trap}}(x, y, z) + g|\psi(x, y, z)|^2)\Delta t/\hbar$, then we transform ψ into Fourier space as $\phi(k_x, k_y, q_z)$ and rotate in complex phase per wavevector site with the calculated dispersion $iD_{V_L, \omega, \xi_{\text{max}}}(\mathbf{q} = (k_x, k_y, q_z))\Delta t/\hbar$. The time step Δt is chosen to be $0.02 \cdot \hbar/E_R$ so that it is sufficiently small. We record the ψ and ϕ at selected time points for further analysis.

For each recorded frame, if the ϕ indeed shows the two-cluster distribution, we acquire the trajectory parameters Δq and θ_q by separating $\phi = \phi_+ + \phi_-$, where $\phi_{\pm}(q_z \lesseqgtr 0) = 0$. Then the center of mass of each segment is calculated. The limitation of this method is that in the case of small or no separation, a small non-zero value is still computed, but this does not prevent useful comparison of the simulation with the experiment.

- [1] Y. Chen, T. T. Georgiou, and A. Tannenbaum, Optimal transport for gaussian mixture models, IEEE Access **7**, 6269 (2018).